Journal of Optics

Imaging the scattering field of a single GaN nanowire

To cite this article before publication: Kaleem Ullah *et al* 2018 *J. Opt.* 20 105608.

https://doi.org/10.1088/2040-8986/aae0d1

Imaging the Scattering Field of a Single GaN Nanowire

Kaleem Ullah [1], Xuefeng Liu [1,*], Lujun Huang [2], Umair Farooq [3], Faisal Iqbal [4], and Braulio Garcia Camara [5]

[1]*School of electronic Engineering and Optoelectronic Technology, Nanjing University of Science and Technology, Nanjing, 210094, Jiangsu, China.*

[2]*Department of Material Science and Engineering, North Carolina State University, Raleigh, NC, 27606.*

[3]*Beijing Key Laboratory of Nanophotonics and Ultrafine Optoelectronic Systems, School of Physics, Beijing Institute of Technology, Beijing 100081, China.*

[4]*Hefei National Laboratory for Physical Science at the Microscale, University of Science and Technology of China, Hefei 230026, China.*

[5]*Group of Displays and Photonic Applications (GDAF-UC3M). Carlos III University of Madrid. Leganes, 28911 Madrid, Spain.*

*liuxf1956@163.com

Abstract

In this work, a single gallium nitride (GaN) nanowire has been examined by our previously reported technique parametric indirect microscopic imaging (PIMI). Mapping of the nanoscale scattering signals from GaN nanowire has been achieved with PIMI system. A comparison with classical far field microscopy and FDTD simulations is included to show the relevant differences and the strength of this technique. In PIMI, highly defined modulated illumination, far field variation quantification, and filtering process resolve nanoscale scattering field distribution in the form of polarization parameters. We believe that our system provides us a platform to understand the physics of these nanoscale scattering fields from optical nanoantennas.

Keywords: Scattering, nanowires, nano-scale, polarization modulation.

Introduction

The development in the fabrication of nanomaterials at optical regime has led to light manipulation at the nanoscale exhibiting novel phenomena such as negative or zero refractive index, optical cloaking and superluminal phenomena [1–3]. These nanoscale scattering field architectures

constitute a promising platform to explore the fundamental physical origin of these novel unprecedented artificial behaviors. Therefore, a reliable imaging technique must be able to map these localized nanoscale scattered fields. In conventional optical microscopy, the diffractive nature of light poses a fundamental limitation on the resolution of electromagnetic wave-based imaging systems [4–10]. Thus, we cannot resolve the scattered field below diffraction limit which is equal to the half of the incident wavelength [11–16]. A continuing effort to develop the existing and new techniques is needed to harness the benefits of optical far field microscopy for ultra-resolution imaging [17–21].

Scanning near field optical microscopy (NSOM) is usually used to map the nano-localized field. NSOM utilizes an optical antenna to convert the electromagnetic near-field into propagating radiation and vice versa [22–26]. However, NSOM is difficult to operate in non-invasive mode and only limited to the surface imaging. Furthermore, its mapping area with subwavelength features is narrow which prevents it to image the sub-diffraction scattering field to a wider range [27]. Several super- and hyperlenses also can achieve the nanometric resolution by utilizing the evanescent field spectrum. However, a detailed study illustrated that resolving capability of these lenses is significantly weakened by the material loss due to the resonant nature of the evanescent waves [28]. Furthermore, the focusing of the evanescent field cannot be achieved with the conventional optics [28–33]. Electron energy-loss spectroscopy (EELS) also can resolve the scattering field with a nanometric accuracy by measuring the change in kinetic energy of electrons after they have interacted with a specimen [34]. Some of the electrons will undergo inelastic scattering, which means that they lose energy and have their paths slightly and randomly deflected [35]. The amount of energy loss can be measured via an electron spectrometer and interpreted in terms of the energy loss. EELS in a scanning transmission electron microscope (STEM) is an essential tool for nanophotonics due to its ability to probe scattering near field at nanometric scale [36]. But in EELS, high energy electron beams can damage the sample under test (SUT). EELS is costly, and required high vacuum conditions, and it is applicable only for thin samples that are transparent to electron beams [35].

Several works have been reported on mapping the scattering field with nano-metric accuracy in plasmonic nanowires [37–52]. Researchers used different imaging methods to map the surface plasmon modes from metallic nanowires, such as NSOM [53], sub-nanometer electron probe [54], two-photon polymerization [55], tip-enhanced Raman spectroscopy [56], etc. In addition to

plasmonic nanowires, semiconductor nanowires, such as GaN nanowires, have been studied due to the enhanced light coupling, directional and polarized scattering at resonant wavelengths [57–60]. In this work, we apply PIMI to image the nano-sized scattering localized modes of a single GaN nanowire, which is the first time to our best knowledge. PIMI is a wide field super-resolution technique which allows us to image the optical modes of the SUT with nanometer accuracy [61, 62]. In PIMI, a linearly polarized beam of light is modulated in a controlled manner. This linearly polarized light excites different scattering information from the SUT and produces changes in the far field point spread function (PSF) due to near to far field coupling. The obtained data in the imaging plane is then fitted using Jones paraxial propagation model [63]. All unnecessary diffraction produced by the neighboring objective field points are filtered off resulting in a reduction of the width of the PSF. In this way, we become able to differentiate between two closely situated points, in particular, we can resolve the scattering modes into the nanoscale region [62]. Several methods have been reported which based on polarization modulation and fitting process to increase the resolving power of their system [63, 64]. In comparison to these methods [63, 64], our proposed method is different in two ways. First, in our post-processing algorithm, our method enables to calculate the Stokes parameters with the interconnection of Jones and Muller models. Second, the controllability of our method on parameters like the modulation speed, the quantification of the far field variation and filtering off the extra diffraction makes our method being able to image the sub-diffraction scattering field information.

Theoretical and Experimental Basis

Any SUT is called optically anisotropic when the refractive index varies with the direction of vibration of light. The anisotropy arises from the directionality of atomic or molecular arrangements in the material [63]. When a linearly polarized light with different polarization angles impinges on the SUT, different anisotropic near field scattering information is excited. The coupling of these near field features with the far field induces a change in the shape of the far field PSF [61, 62]. That is why, depending on the anisotropy exhibited by the SUT, different shapes of the PSF appeared in the imaging plane. PIMI is a home-built system made by modifying the BX51 Olympus microscope [61, 62]. A schematic of the PIMI system is displayed in Fig. 1(a). In PIMI method, these far field PSF changes have been quantified under the goodness of the fit. After

removing the unwanted scattering produced by the neighboring field points, we become able to bring the extra scattering and structural information of the sample [62].

A linearly polarized light with different polarization angles propagates towards the SUT as shown in Fig. 1(a). When this linearly polarized light interacts with the SUT, it excites the scattering modes, which vary with the polarization angle of the incident wave. Various kinds of scattering information enabled by the SUT-light interaction with different polarization angles have been represented with the colored arrows. The black arrow represents the scattering modes information enabled by polarization angle equal to 0°, while the red, blue and green arrows correspond to 45°, 90°, and 135°, respectively.

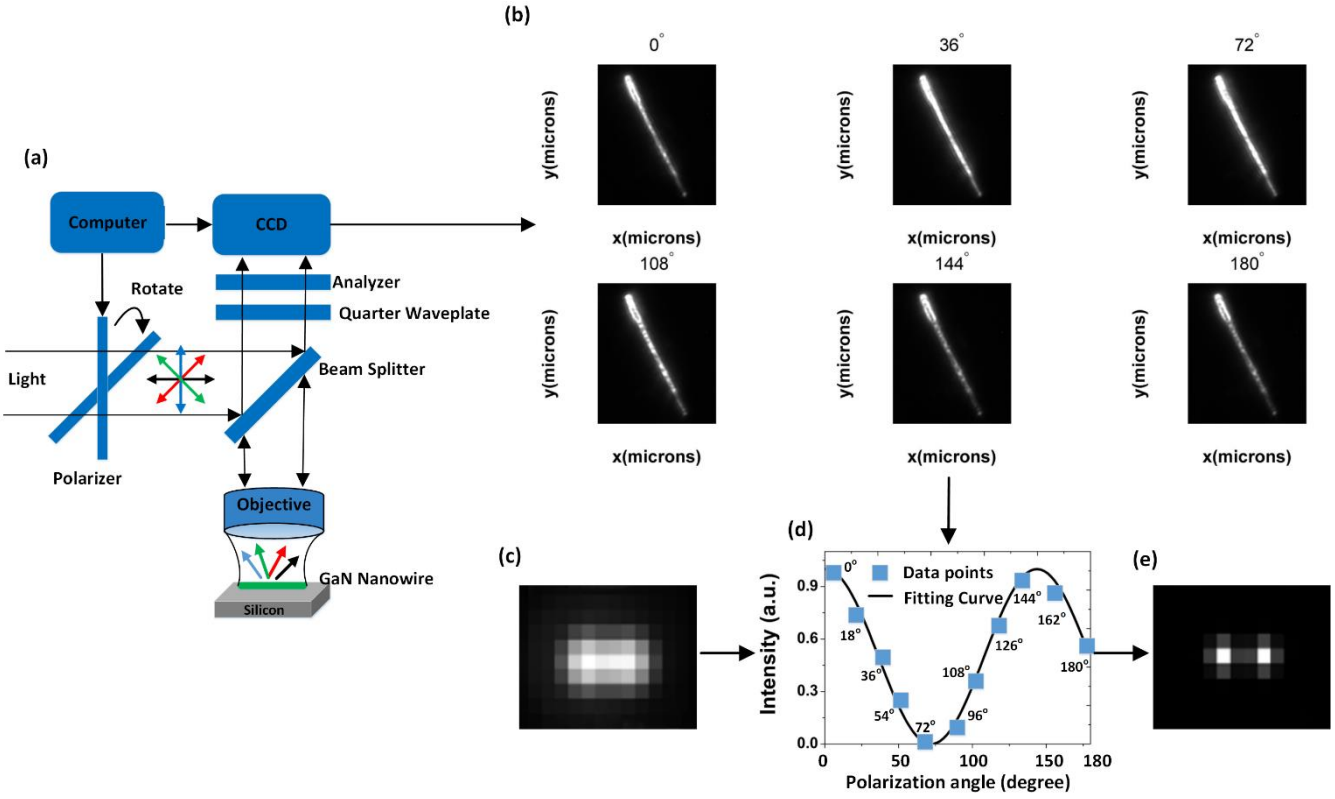

Figure 1. (a) A representation of the excitation of linearly polarized light under the normal incidence of light in the PIMI system. This linearly polarized light excites different scattering modes information indicated by different colors of the arrows. (b) Scattering field distribution in gray scale color using dark field PIMI with 100x objective of the numerical aperture of 0.90. The wavelength used was 532 nm. (c-e) A representation of how PIMI perform fitting operation, and how after removing the unwanted scattering from the neighboring field points, the width of the PSF decreases and we become able to differentiate between two close points.

As expected, the measured scattering distribution of a single GaN under the dark field illumination in PIMI system collects different scattering information as can be visualized from Fig. 1(b). This can be observed well from the scattering distribution appeared both inside and outside of the GaN nanowire as displayed in Fig. 1(b). In PIMI system, we usually modulated the incident field from 0^o to 360^o with an angle period of the 18^o. This means we get 20 pictures captured by the detector in every measurement. The pixel intensity in the imaging plane can be described mathematically by the given Jones model [63,64].

$$I = \frac{I_0}{2}[1 + \sin 2(\alpha - \phi)\sin\delta] \tag{1}$$

Where I_0 is the un-polarized intensity, α is the rotational angle of the polarizer, ϕ is the angle along the slow vibration axis and δ is the optical retardation (phase shift between the E_y and E_x).
By expanding equation (1) trigonometrically, we get:

$$I = \frac{1}{2}I_0 + \frac{1}{2}I_0 \sin\delta\cos 2\phi \sin 2\alpha - \frac{1}{2}I_0 \sin\delta \sin 2\phi \cos 2\alpha \tag{2}$$

The derivation of the quantities of interest is achieved by a least-squares fitting procedure to the following equation:

$$I = a_0 + a_1 \sin 2\alpha + a_2 \cos 2\alpha \tag{3}$$

By comparing equations (2) and (3), the parameters are obtained:

$$a_0 = \frac{1}{2}I_0, a_1 = \frac{1}{2}I_0 \sin\delta\cos 2\phi, a_2 = -\frac{1}{2}I_0 \sin\delta \sin 2\phi \tag{4}$$

By rotating the polarization angle (α) along a complete circumference with a resolution of 18º, a total number of angles N= 20 and a_0, a_1 and a_2 are calculated as:

$$a_0 = \sum_{i=1}^{N}\frac{1}{N}I_i, \quad a_1 = \sum_{i=1}^{N}\frac{2}{N}I_i \sin 2\alpha_i, \quad a_2 = \sum_{i=1}^{N}\frac{2}{N}I_i \cos 2\alpha_i \tag{5}$$

In equation 5, the subscript "*i*" denoted the different angles of the polarizer i.e. i= 0º, 18º, … 180º while I_i corresponds to the intensity of the incident field at those polarization configurations. Using these parameters, the desired quantities can be found as:

$$I_{dp} = a_0, \sin\delta = \frac{(a_1^2 + a_2^2)^{\frac{1}{2}}}{a_0}, \phi = \frac{1}{2}\arcsin\left(-\frac{a_2}{(a_1^2 + a_2^2)^{\frac{1}{2}}}\right) \quad (6)$$

And then, Stokes parameters can be calculated by a mutual relationship between Jones and Muller model as follows:

$$\begin{aligned} S_0 &= I_{dp}(1+\sin\delta) = E_{0x}^2 + E_{0y}^2 \\ S_1 &= I_{dp}(1+\sin\delta)\cos 2\phi = E_{0x}^2 - E_{0y}^2 \\ S_2 &= 2\sqrt{I_{dp}}(1+\sin\delta)\cos 2\phi = 2E_{0x}E_{0y}\sin\delta \\ S_3 &= 2\sqrt{I_{dp}}(1+\sin\delta)\sin 2\phi = 2E_{0x}E_{0y}\cos\delta \end{aligned} \quad (7)$$

After obtaining the data for all polarization angles, the fitting and filtration process at each pixel in the imaging plane has been performed by utilizing the fitting equation 3. A representation of the fitting curve has been shown in Fig. 1(d). Only the central spatial points of the field spot confirm the near field anisotropic coupling to far field and hence fit well with the fitting criteria such as adjusted-root-square [62]. These points are called authentic points whereas other points have been filtered out as noise. Figure 1(c-e) indicates that how the diffraction limited points are resolved with the fitting process in the PIMI.

After filtering off the unwanted scattering signals, the width of the PSF decreases and we become able to differentiate between two closely situated points as can be seen from Fig. 1(e). After the curve fitting process, the derived quantities such as I_{dp}, which is the average of all polarization intensities, sinδ and ϕ can be obtained offering a mapping of the scattering distribution, which cannot be possible to image with conventional microscopy. With the use of these derived quantities, Stokes parameters are obtained by the interconnection of Jones and Muller model as represented in equation (7). These all indirect PIMI parameters resolve the scattering field distribution differently. Every parameter define the scattering and structural characteristics of the SUT in a different manner. These indirect parameters not only explain the scattering and structural information of the SUT but also reveal a complete polarization status of the scattering field.

Experimental setup of the PIMI

PIMI is a wide field home build system made by modifying an Olympus BX51 conventional microscope which provides the basic optical light path. We incorporated a modulator that consists of a motor and linear polarizer. This modulator having a precise control and able to rotate the linear polarization of incident light with a precision of 0.05 degree. A quarter wave plate and an analyzer also inserted in front of the imaging plane as can be observed by the Fig. 1(a). A Basler CCD (PiA2400-17gm) is used to collect the light. This CCD consists of 5 million pixels with a pixel resolution 3.45 microns. This CCD can obtained a resolution of 34.5 nm with a 100x objective if the diffraction limit is broken and Nyquist principle is fulfilled. Direct and indirect data was analyzed by the ANISOSCOPE software [62].

Results and Discussion

GaN nanowires were synthesized using a cost-effective method [65,66]. The scanning electron microscopic (SEM) characterization was done to analyze the structural and morphological details. SEM micrographs of the nanowires have been displayed in Fig. 2. In the inset, at the top left corner of the image shown in Fig. 2, the higher magnification image has been displayed which shows nice structural details of the GaN nanowire. We dispersed the GaN nanowires on the silica substrate in this way that they become separated from each other. A distance of several micrometers was created between the nanowires so that we can study the scattering of a single nanowire and avoid the scattering effect by the neighboring nanowires. Fig. 2(b) represents the conventional microscopic result of the single nanowire under observation. The boundary of the wire is represented by a dashed line. This single nanowire does not exhibit a totally uniform diameter, instead, it is higher in the upper area as can be observed from the Fig. 2(c). After 3 μm length, its diameter becomes 500 nm and then again turns to narrow at the end of the nanowire as can be seen from the Fig. 2(c). A spherical shape like boundary appears at the end of the nanowire and the total length of the nanowire is about 17 μm.

A single GaN nanowire is probed under the dark and bright field illumination of the PIMI system. A comparison with the conventional microscopic (*CM*) result is displayed in order to confirm the PIMI nanoscale mapping. The images of the PIMI indirect parameters are provided in Fig. 3 along with the *CM* image. The color bar is normalized for the comparison purpose. The width of the wire changes from 600 nm to 250 nm approximately as can be observed from the Fig. 3. In *CM* image, the edge irregularities are not well resolved whereas, in the $sin\delta$ image, these are very well resolved

as can be visualized from Fig. 3(c). There is an excitation of the several localized modes inside the wire which are also can be seen in the *sinδ* image. It is worth noting that I_{dp} itself did not provide enough edge information of the wire, however, it still reflected better edge information as compared to the *CM*. Furthermore, some of the localized modes in the middle of the wire are resolved by I_{dp}.

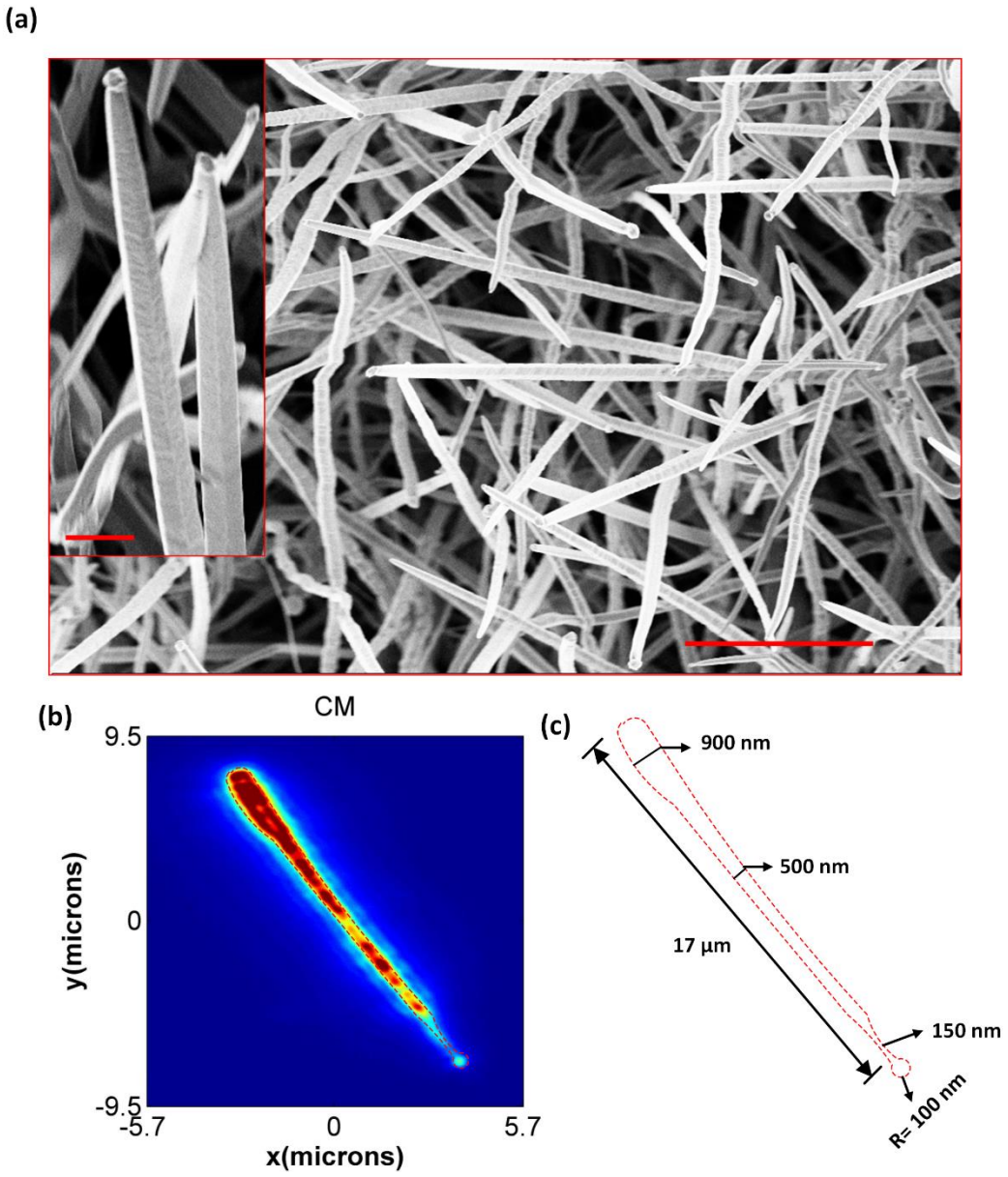

Figure 2. (a) Scanning electron microscopic (SEM) image of GaN nanowires, the length of the scale bar for the image shows many GaN nanowires is equal to 10 microns, whereas, in the inset of the image at the top left it is equal to 1 micron. (b) The conventional microscopy result captured

by 100x objective of the numerical aperture of 0.90. The boundary of the nanowire is marked by a red dashed line. (c) The dimensions and geometry of the GaN single nanowire is shown which used in the experiment.

The PIMI parameter ϕ conveyed us the scattering field information to a much larger range comparing to the *CM* image, which is given by the Fig. 3(d). Very close to the edge of the wire at the head of the wire, we found the fringes of the scattering field with higher frequency. These high frequency fields exhibit the information of the evanescent field which is not present in *CM*. The frequency of these fringes is not higher but at the top side of the wire, in ϕ image, higher frequency fringes of the scattering field can be observed as shown in Fig. 3(d).

We also mapped the scattering field distribution of a single GaN nanowire in terms of the Stokes parameters. These Stokes parameters are highly desired in describing the polarization status in many applications, such as singular optics, optical nanoantenna etc. PIMI provides us a platform to calculate the Stokes parameters with sub-diffraction scattering field information. Stokes S_0 parameter shows fine details of the localized modes inside the GaN nanowire as can be seen from Fig. 3(e). Similarly, optical mode mapping at the center of the nanowire portion is visualized by the S_1 parameter. At the same time, the morphological information at the upper side of the nanowire is resolved by the S_1 parameter. S_2 and S_3 also carried scattering modes information as well as the structural information of the nanowire. Furthermore, from Fig. 3(e-h), we can find that at the lower portion of the GaN nanowire, the localized field resolved by PIMI Stokes parameters have a smaller size as compared to the *CM* image.

We plotted the intensity values by extracting the data in terms of a line parallel to the axis along the length of the nanowires as can be observed from the Fig. 4(b, c). At the same position, same length line data has been plotted for both indirect PIMI parameters and *CM* in order to compare the spatial signatures. In the *CM* line graph, The intensity has a plateau in the area of the nanowire, and it decreases exponentially to zero after a little distance as can be observed from the Fig. 4(a). I_{dp} also shows the same pattern of the scattering distribution as of *CM*. Stokes parameters provide scattering information at spatial positions where *CM* results give an almost null signal as can be seen in Fig. 4(a). The spatial signature of every Stokes parameter is different because they deliver different polarization characteristics of the scattering light from the GaN nanowire. In Fig. 4(a), several nano-sized localized fields can be observed in the PIMI indirect parameters such as $sin\delta$ and S_0,. That is because, in these parameters, the half width at full maximum (HWFM) is in the

nano-sized as can be observed from the line graphs of the $sin\delta$ and S_0 result presented in the Fig. 4(a). The spatial signature of the PIMI parameter ϕ is different from other parameters because it only provides the scattering information outside of the GaN nanowire.

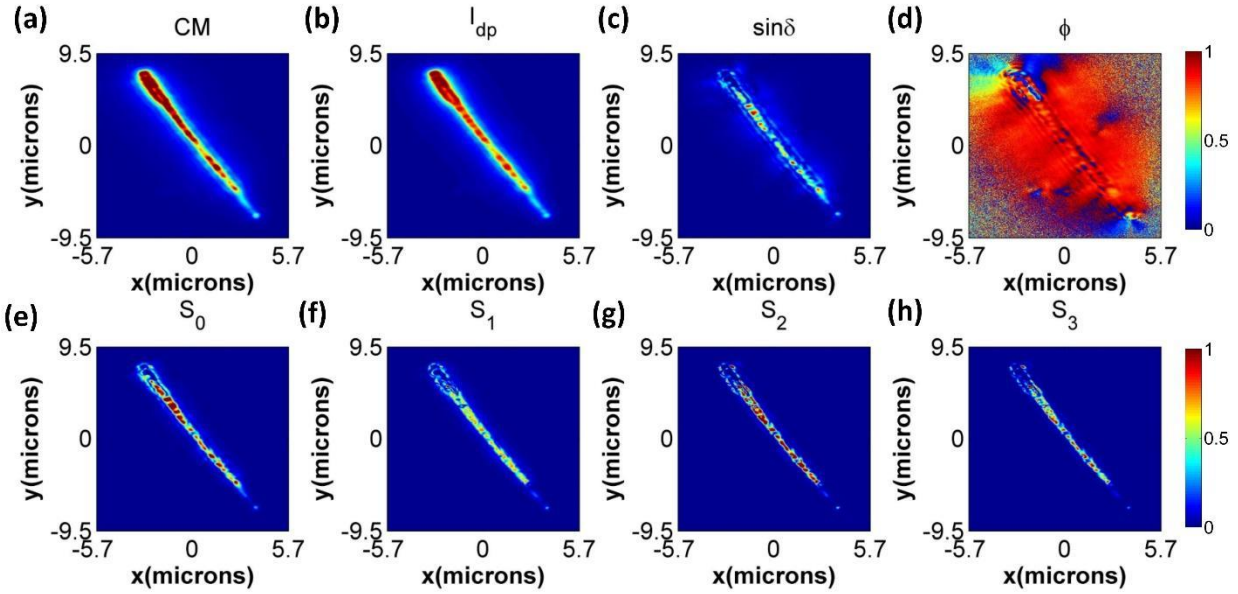

Figure 3. (a) Conventional optical microscopic image delivered by dark field PIMI system using 100x objective of the numerical aperture of 0.90 at wavelength 532 nm. (b-h) PIMI parameters using the same optics as used in (a).

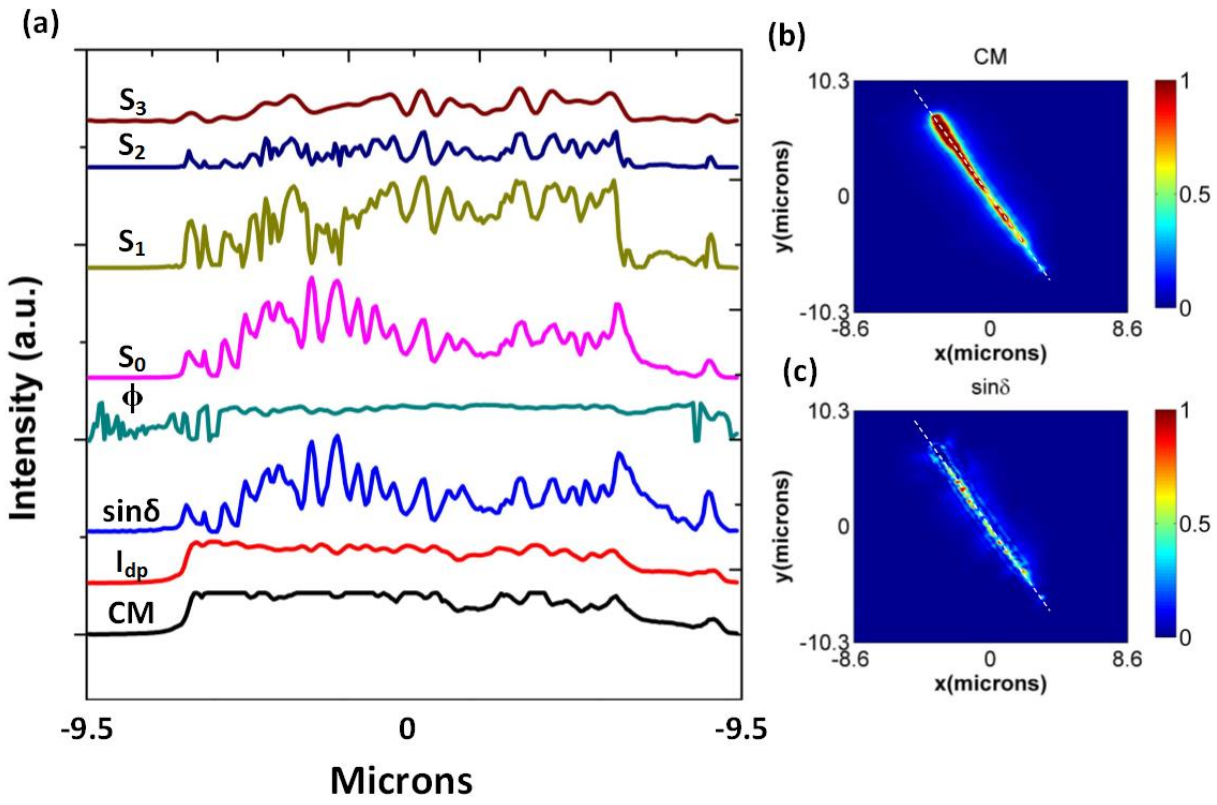

Figure 4. (a) Intensity values are plotted in the form of line graph of all indirect PIMI parameters and the conventional microscopic (*CM*) result. The intensity data is extracted in the form of a line showed in (b) *CM* image (c) *sinδ* image.

We also plotted the intensity values extracted in the form of a line perpendicular to the length axis of the GaN wire as can be seen from Fig. 5(b, c). In case of *CM*, there is no scattering information available away from the edge of the nanowire. The scattering field trend in the I_{dp} and Stokes parameters is also the same as that in*CM,* as can be seen in Fig. 5(a). However, the trend of sensing the scattering signal is different in *sinδ* and ϕ parameters curve, as can be also seen in Fig. 5(a). The line intensity curve in terms of *sinδ* presents the detection of the scattering signal at that point where the *CM* graph showed a null value. This means that the range of the scattering signal in the *sinδ* parameter is higher. The most sensitive parameter in this regard is ϕ. The scattering range presented by ϕ is the largest and almost 4 to 5 times more than that of the CM result, (see Fig. 5(a)). In ϕ image, we also detected some higher frequency near field fringes which confirms the higher sensitivity of this parameter as can be visualized from Fig 5(a).

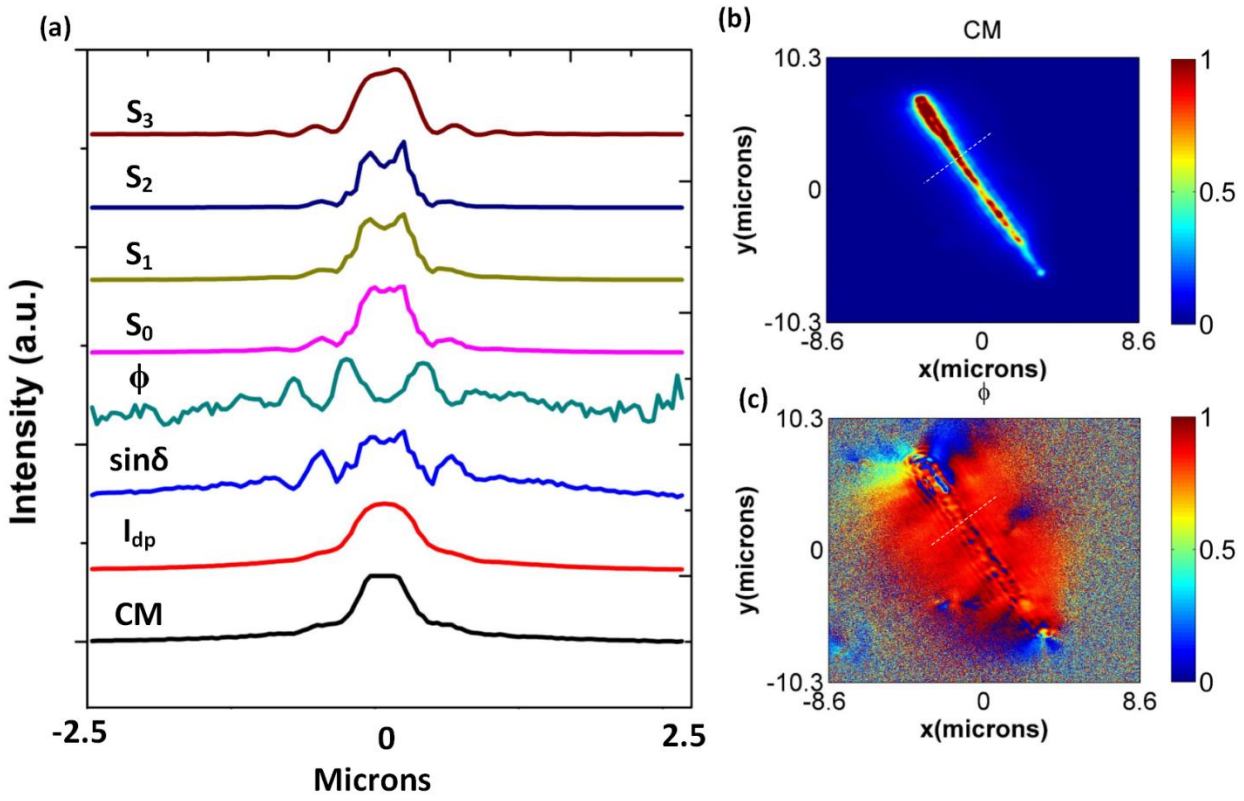

Figure 5. (a) Intensity values plotted in the form of the line graph of all indirect parameters and conventional microscopic (*CM*) result. These intensity values extracted in terms of a line showed in (b) *CM* image (c) ϕ image.

We also mapped the same single GaN in the illumination of the bright field PIMI as shown in Fig. 6. It can be found that the *CM* just resolved the upper portion of the nanowire in a satisfactory level, while leaving the lower portion non-resolved. There is no information of the scattering field inside the GaN nanowire, as can be visualized from the Fig. 6(a). I_{dp} at this time showed a little variation as compared to the *CM* and resolved some optical modes at the lower portion of the nanowire as can be seen from Fig. 6(a, b). Moreover, I_{dp} also resolved the localized field appeared at the lowest part of the GaN nanowire lacked by the *CM* as can be visualized with a comparison of the Images of *CM* and I_{dp}.

Sinδ records a well-resolved mapping of the optical modes in the GaN nanowire as can be visualized from Fig. 6(c). PIMI indirect parameter ϕ presents structural characteristics of the GaN in an excellent way as can be seen from the Fig. 6(d). The Stokes S_0 parameter also conveys us optical modes information as the indirect parameter *sinδ* did. Similarly, PIMI stokes parameters S_1

and S_2 also resolves the scattering distribution inside the GaN nanowire, but resolving of the optical modes in the GaN is not as clear as in the S_0 and $sin\delta$. The structural and scattering details along with the subwavelength chirality scattering distribution are presented by S_3 parameter because it is equal to the differential intensity between the LCP and RCP light. The bright field PIMI indirect parameters together with the *CM* are presented in Fig. 6 show that PIMI resolves the localized field and structural details inside the GaN nanowire, especially in the ϕ, $sin\delta$ and S_0 parameters in a much finer way as compared to the *CM* image. Also, it can be analyzed that PIMI indirect parameters resolved a lower portion of the GaN nanowire which is very thin and the localized field appeared in the lowest part of the nanowire as can be observed comparing Fig. 6 (a) and (b-h).

We plotted the intensity profile of direct conventional microscopic result and our indirect PIMI parameters result in the form of line graph. The data of these line graphs plotted in Fig. 7(a) has been extracted in terms of a line parallel to the length axis of nanowire as represented in Fig. 7(b, c). As can be seen, as usual, there is no scattering distribution except the upper portion of the wire in the *CM* image. In the middle of the wire, the optical modes information is unclear in *CM* result. The I_{dp} curve is different from the *CM* curve especially in the middle of the nanowire portion. Similarly, the line plot of the $sin\delta$ also shows enough scattering peaks at an inner portion of the wire. All the Stokes parameters also present prominent peaks at the position where the *CM* curve presented negligible value as can be analyzed from the Fig. 7(a). This proves the sensitivity of the PIMI indirect parameters. As expected, the ϕ curve contains more peaks and detected the weak and strong scattering signals that can be observed by comparing its curve with *CM* curve.

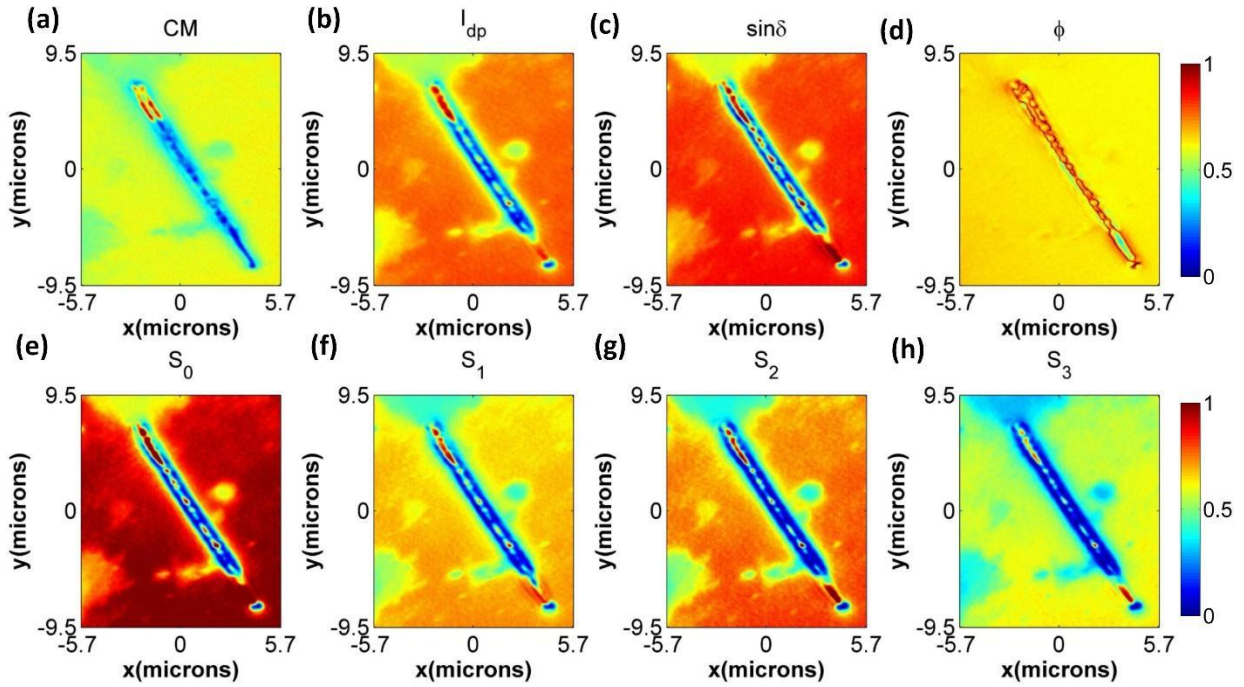

Figure 6. (a) Conventional optical microscopic image delivered by bright field PIMI system using 100x objective of the numerical aperture of 0.90 at wavelength 532 nm. (b-h) PIMI parameters using the same optics as used in (a).

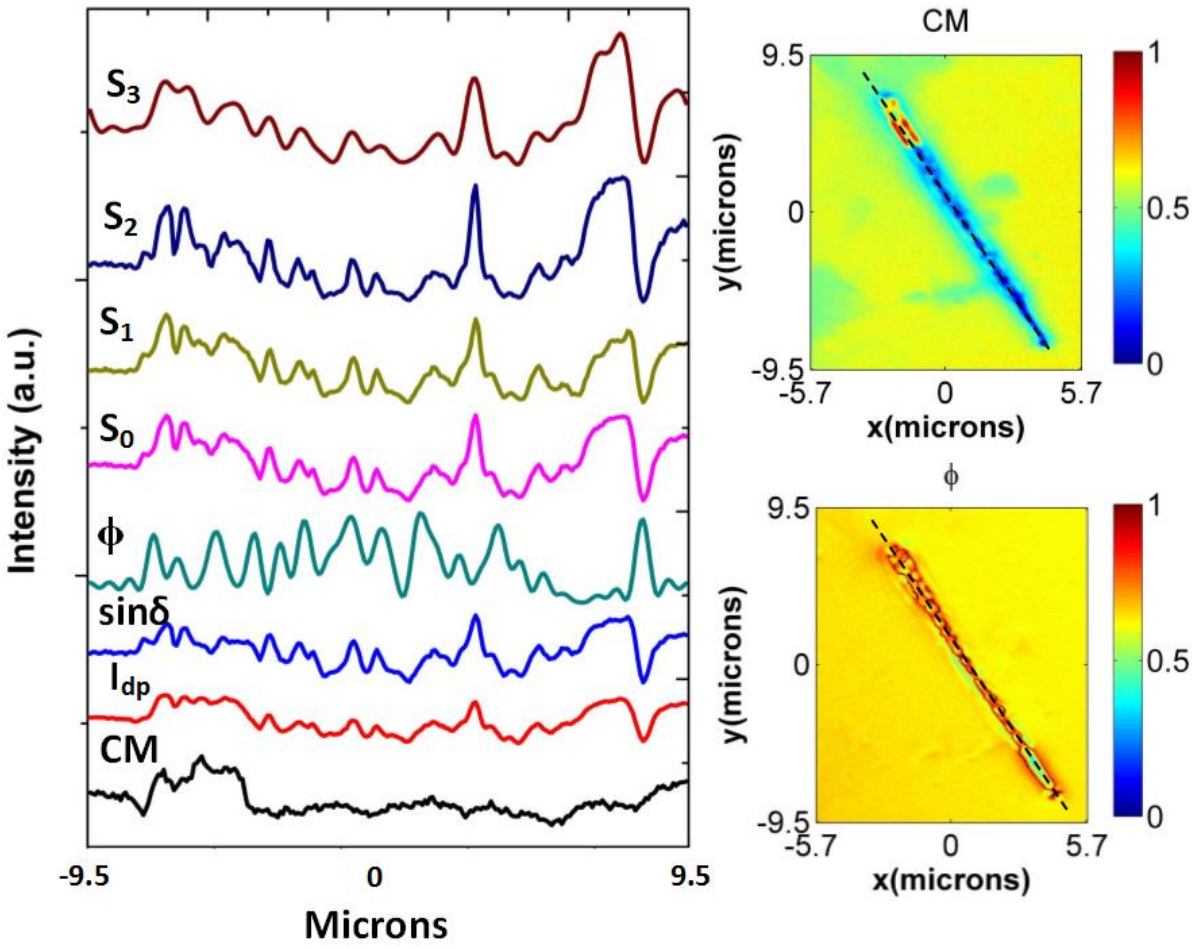

Figure 7. (a) Line graph representation of the conventional optical microscopic intensity and spatial profiles of all PIMI indirect parameters. (b, c) The data extraction representation in the form of a line parallel to the length axis of the GaN nanowire.

In order to confirm the nanoscale ability of our system PIMI, we simulated the scattering field inside the GaN nanowire using FDTD method. For this purpose, we set up the model according to the experimental conditions. A schematic of the light illumination on the nanowire has been illustrated in Fig. 8(d). Firstly, we calculated the magnitude of the scattering electric field by using equation (7). After that, we selected the middle portion of the nanowire because it has the highest uniformity along the wall of the nanowire and good for the comparison with simulation result delivered by the FDTD method. The scattering electric field delivered by PIMI method is displayed in Fig. 8(a). We magnified the selected area indicated by the dashed rectangle in Fig. 8(a). This selected area is shown in Fig. 8(b). The corresponding simulation area of the nanowire delivered

by the FDTD method is also displayed in Fig. 8(c). If we compare the Fig. 8(b & c), then we will come to know that several nano-sized localized fields can be viewable in PIMI result of scattering electric field indicated by the small arrows in Fig. 8(b). Our FDTD near field simulation also proved the same spherical nano-fields within the boundary of the nanowire as also indicated by the small arrows in Fig. 8(c). From the simulation, result provided in Fig. 8(c), it has been proved that our PIMI method has the ability to map the nano-sized scattering field, which is lacked by the conventional microscopy. The difference between the PIMI and FDTD result may lie because in simulation, we sliced the particle into a plane whereas, in PIMI, we cannot do that. Moreover, there is also some non-uniform boundaries of the nanowire which is not included in the simulation model.

In dark field PIMI parameter ϕ, we detected the scattering range which has larger scattering area as compared to the *CM* image as can be observed by Fig. 9(a, d). We plotted the dashed rectangular area of images of *CM* and ϕ in Fig. 9(b, e) in order to compare scattering and structural details between *CM* and ϕ. In the larger ranged scattering area of the ϕ, we detected high-frequency field fringes as indicated by the arrows symbol in Fig. 9(e). It is also noticeable that ϕ also provided the structural details like non-uniform edges and surface roughness of the GaN nanowire as indicated by the arrows, whereas, this information is lacked by the *CM* as can be observed by the comparison of Fig. 9(b, e).

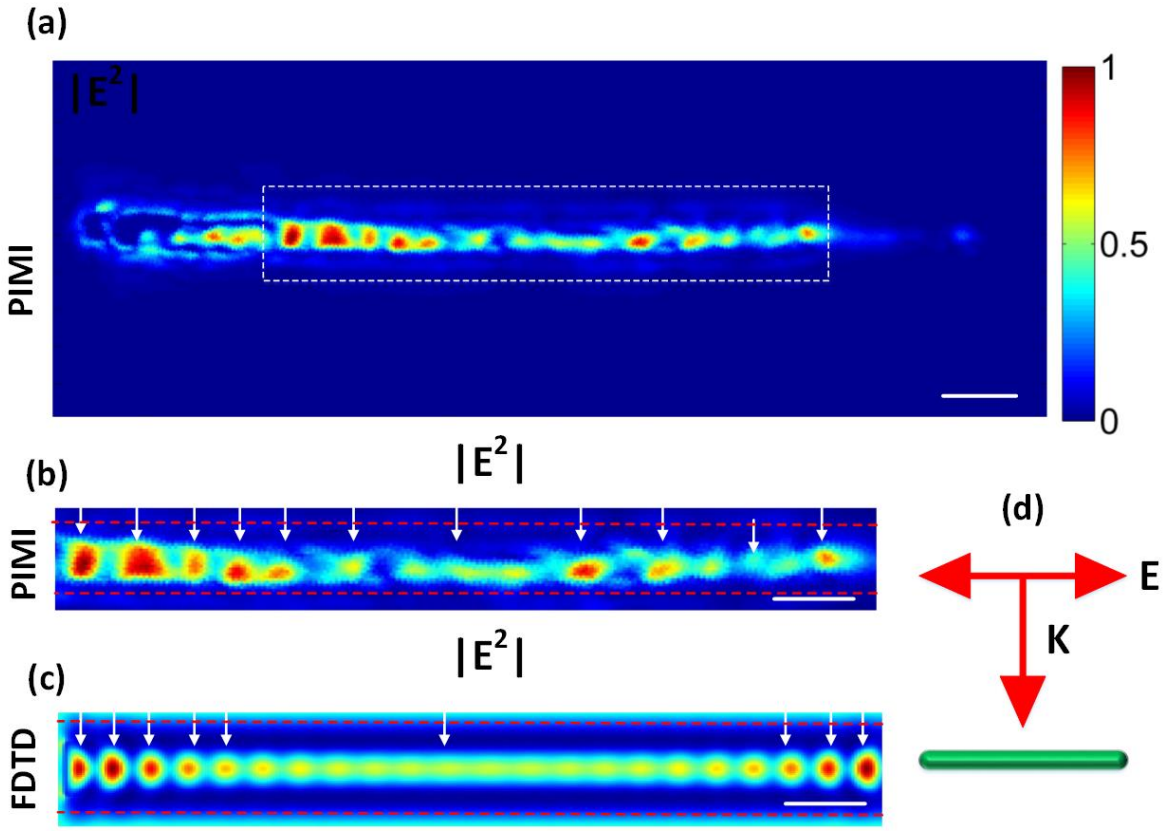

Figure 8. (a) Scattering electric field from PIMI system calculated using equation (7). (b) The selected area indicated by the dashed rectangle in (a). (c) The simulation result of the scattering near field delivered by the FDTD method. (d) The schematic of the light illumination used in the simulation model. The length of the scale bar is of 1 micron.

We also plotted the intensity profiles of *CM* and PIMI indirect parameters ϕ by extracting the data along a line perpendicular to the length axis of the nanowire as displayed in Fig. 9 (b, e). As can be seen from the Fig. 9(c, f), the *CM* curve resolve only one point within the plotted data whereas our PIMI parameter ϕ resolved two points within that region. Moreover, intensity is exponentially decay and approaches to zero after covering 2 micron distance in CM line graph indicated by arrow symbol provided in Fig. 9(c). Whereas, this trend is not followed by the ϕ image and we get the scattering signal value even after the 2 micron distance from the nanowire boundary as can be observed from the Fig. 9(f). This proved the ability of PIMI parameter ϕ to sense the scattering signals to a larger range as compared to the *CM* result [62]. This extra scattering in PIMI method

provides us a way to recover the extra structural details of the sample such as its edges, boundaries etc. which cannot be possible in the conventional microscopy.

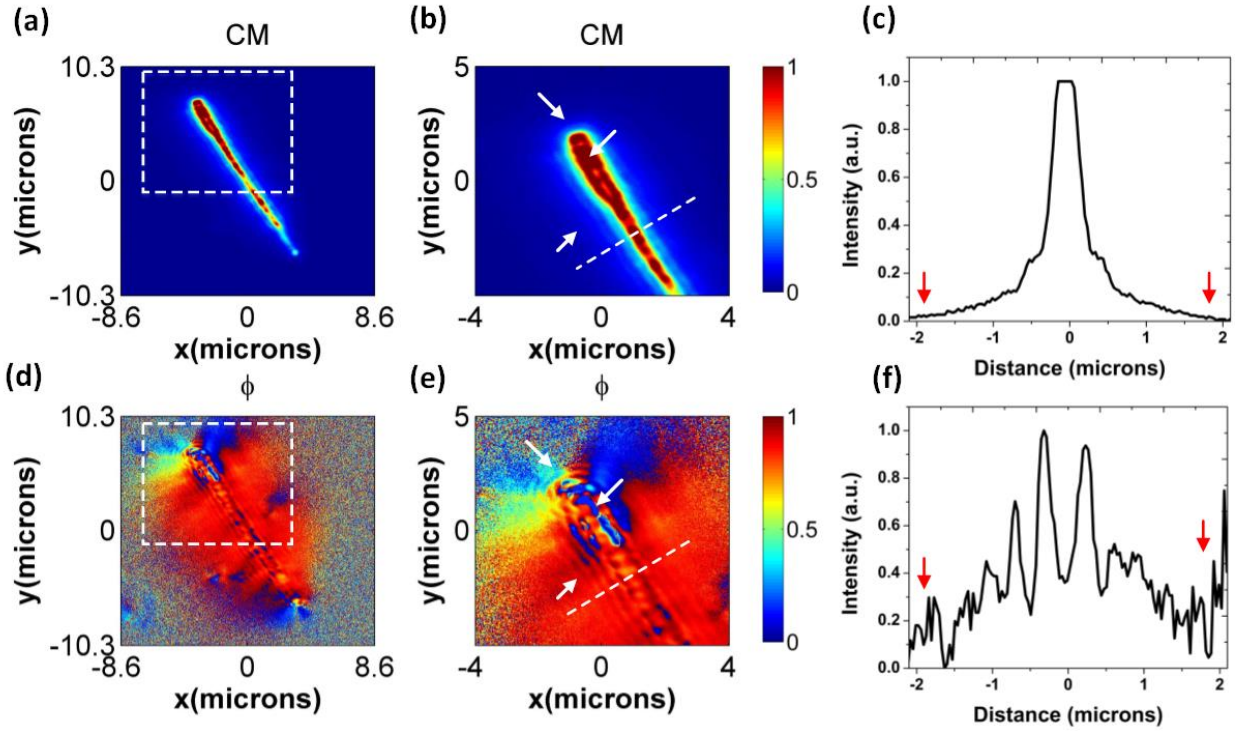

Figure 9. (a) Conventional microscopic result under dark field illumination using 100x objective of the numerical aperture of 0.90. (b) The magnified figure of the *CM* result as indicated by the dotted rectangle in (a). (c) The intensity graph plotted for the data extracted in the form of the line indicated in (b). (d) Similarly, the PIMI indirect parameter ϕ mapped with the same optics as applied for *CM* result in (a). (e) The magnified area indicated by a rectangular dashed in (d). (f) Line graph of the intensity of the data extracted from (e) in the form of a line.

Conclusion

We successfully imaged the nanoscale scattering signals from the GaN nanowire by applying PIMI method. We compared this nanoscale mapping delivered by the PIMI with the conventional optical far field microscopy. PIMI resolved the scattering field distributions 3 to 4 times greater than that of conventional microscopy. We also confirmed the nano-scale scattering field mapping ability of the PIMI system with FDTD near field simulations. Dark field PIMI parameter ϕ resolved scattering distribution to a larger visualization area as compared the scattering range delivered by

conventional microscopy. The indirect parameters of the PIMI not just resolved the nanoscale scattering information but also delivered a complete polarization status of the scattering field from the sample under test. Thus, PIMI is a promising alternative to conventional microscopy and equivalent to other polarimetric techniques with a remarkable difference of the filtering method, providing extra information about the structural properties of the samples.

Acknowledgement

The authors wish to acknowledge the financial support National Key Research and Development Program of China (2017YFF0107100), National Natural Science Foundation of China (NSFC) (61501239), NSFC-2017 (International Young Scientist Research Fund no. 61750110520) and the "Zijin Professor Project" of Nanjing University of Science and Technology. BGC wants to thank the financial support from Agencia Estatal de Investigación and FEDER for the Project TEC2016-77242-C3-1-R AEI/FEDER, UE and Comunidad de Madrid for the SINFOTON-CM Research Program (S2013/MIT-2790).

References

[1] Liu N, Weiss T, Mesch M, Langguth L, Eigenthaler U, Hirscher M, Sönnichsen C and Giessen H 2010 Planar metamaterial analogue of electromagnetically induced transparency for plasmonic sensing *Nano Lett.* **10** 1103–7

[2] Cai W, Chettiar U K, Kildishev A V. and Shalaev V M 2007 Optical cloaking with metamaterials *Nat. Photonics* **1** 224–7

[3] Kivshar Y S 2015 Metamaterials, metasurfaces, and metadevices *Aust. Phys.* **52** 47–50

[4] Huang B, Babcock H and Zhuang X 2010 Breaking the diffraction barrier: Super-resolution imaging of cells *Cell* **143** 1047–58

[5] Zheludev N I 2008 What diffraction limit? *Nat. Mater.* **7** 420–2

[6] Hell S W 2010 Far-field optical nanoscopy *2010 23rd Annu. Meet. IEEE Photonics Soc. PHOTINICS 2010* **1153** 3–4

[7] Mortensen K I, Churchman L S, Spudich J A and Flyvbjerg H 2010 Optimized localization analysis for single-molecule tracking and super-resolution microscopy *Nat. Methods* **7** 377–81

[8] Riedl M 2001 Diffraction Limit *Opt. Des. Fundam. Infrared Syst.* **257** 699–700

[9] Wong A M H and Eleftheriades G V. 2013 An Optical Super-Microscope for Far-field,

Real-time Imaging Beyond the Diffraction Limit *Sci. Rep.* **3** 1715

[10] Hirano Y, Matsuda A and Hiraoka Y 2015 Recent advancements in structured-illumination microscopy toward live-cell imaging *Microscopy* **64** 237–49

[11] Betzig E, Patterson G H, Sougrat R, Lindwasser O W, Olenych S, Bonifacino J S, Davidson M W, Lippincott-Schwartz J and Hess H F 2006 Imaging intracellular fluorescent proteins at nanometer resolution. *Science* **313** 1642–5

[12] Montgomery P C, Leong-Hoi A, Anstotz F, Mitev D, Pramatarova L and Haeberlé O 2016 From superresolution to nanodetection: overview of far field optical nanoscopy techniques for nanostructures *J. Phys. Conf. Ser.* **682** 12010

[13] Small A and Stahlheber S 2014 Fluorophore localization algorithms for super-resolution microscopy *Nat. Methods* **11** 267–79

[14] Sheppard C J R 2007 Fundamentals of superresolution *Micron* **38** 165–9

[15] Hell S W and Wichmann J 1994 Stimulated-Emission-Depletion Fluorescence Microscopy *Opt. Lett.* **19** 780–2

[16] Bechhoefer J 2015 What is superresolution microscopy? *Am. J. Phys.* **83** 22–9

[17] Hell S W, Sahl S J, Bates M, Zhuang X, Heintzmann R, Booth M J, Bewersdorf J, Shtengel G, Hess H, Tinnefeld P, Honigmann A, Jakobs S, Testa I, Cognet L, Lounis B, Ewers H, Davis S J, Eggeling C, Klenerman D, Willig K I, Vicidomini G, Castello M, Diaspro A and Cordes T 2015 The 2015 super-resolution microscopy roadmap *J. Phys. D. Appl. Phys.* **48** 443001

[18] Patterson G, Davidson M, Manley S and Lippincott-Schwartz J 2010 Superresolution Imaging using Single-Molecule Localization *Annu. Rev. Phys. Chem.* **61** 345–67

[19] Yildiz A and Selvin P R 2005 Fluorescence imaging with one nanometer accuracy: Application to molecular motors *Acc. Chem. Res.* **38** 574–82

[20] Ober R J, Ram S and Ward E S 2004 Localization Accuracy in Single-Molecule Microscopy *Biophys. J.* **86** 1185–200

[21] Rust M J, Bates M and Zhuang X 2006 Sub-diffraction-limit imaging by stochastic optical reconstruction microscopy (STORM) *Nat. Methods* **3** 793–6

[22] Habteyes T G, Staude I, Chong K E, Dominguez J, Decker M, Miroshnichenko A, Kivshar Y and Brener I 2014 Near-Field Mapping of Optical Modes on All-Dielectric Silicon Nanodisks *ACS Photonics* **1** 794–8

[23] Neuman T, Alonso-González P, Garcia-Etxarri A, Schnell M, Hillenbrand R and Aizpurua J 2015 Mapping the near fields of plasmonic nanoantennas by scattering-type scanning near-field optical microscopy *Laser Photonics Rev.* **9** 637–49

[24] Rotenberg N and Kuipers L 2014 Mapping nanoscale light fields *Nat. Photonics* **8** 919–26

[25] Ullah K, Liu X, Yadav N P, Habib M, Song L and García-Cámara B 2017 Light scattering by subwavelength Cu $_2$ O particles *Nanotechnology* **28** 134002

[26] Rahmani M, Shorokhov A S, Hopkins B, Miroshnichenko A E, Shcherbakov M R, Camacho-Morales R, Fedyanin A A, Neshev D N and Kivshar Y S 2017 Nonlinear Symmetry Breaking in Symmetric Oligomers *ACS Photonics* **4** 454–61

[27] Bettiol A A, Mi Z and Watt F 2016 High-resolution fast ion microscopy of single whole biological cells *Appl. Phys. Rev.* **3**

[28] Jacob Z, Alekseyev L V. and Narimanov E 2006 Optical Hyperlens: Far-field imaging beyond the diffraction limit *Opt. Express* **14** 8247

[29] Lee H, Liu Z, Xiong Y, Sun C and Zhang X 2007 Development of optical hyperlens for imaging below the diffraction limit *Opt. Express* **15** 15886

[30] Wang W, Xing H, Fang L, Liu Y, Ma J, Lin L, Wang C and Luo X 2008 Far-field imaging device: planar hyperlens with magnification using multi-layer metamaterial *Opt. Express* **16** 21142

[31] Wang Y T, Cheng B H, Ho Y Z, Lan Y-C, Luan P-G and Tsai D P 2012 Gain-assisted hybrid-superlens hyperlens for nano imaging. *Opt. Express* **20** 22953–60

[32] Zhang T, Chen L and Li X 2013 Graphene-based tunable broadband hyperlens for far-field subdiffraction imaging at mid-infrared frequencies *Opt. Express* **21** 20888–99

[33] Lu D and Liu Z 2012 Hyperlenses and metalenses for far-field super-resolution imaging *Nat. Commun.* **3** 1–9

[34] Colliex C, Kociak M and Stéphan O 2016 Electron Energy Loss Spectroscopy imaging of surface plasmons at the nanometer scale *Ultramicroscopy* **162** A1–24

[35] Merlen A and Lagugné-Labarthet F 2014 Imaging the optical near field in plasmonic nanostructures *Appl. Spectrosc.* **68** 1307–26

[36] Shekhar P, Malac M, Gaind V, Dalili N, Meldrum A and Jacob Z 2017 Momentum-Resolved Electron Energy Loss Spectroscopy for Mapping the Photonic Density of States

ACS Photonics **4** 1009–14

[37] Sanders A W, Routenberg D A, Wiley B J, Xia Y, Dufresne E R and Reed M A 2006 Observation of plasmon propagation, redirection, and fan-out in silver nanowires *Nano Lett.* **6** 1822–6

[38] Ma Y, Li X, Yu H, Tong L, Gu Y and Gong Q 2010 Direct measurement of propagation losses in silver nanowires. *Opt. Lett.* **35** 1160–2

[39] Sun M, Zhang Z, Wang P, Li Q, Ma F and Xu H 2013 Remotely excited Raman optical activity using chiral plasmon propagation in Ag nanowires *Light Sci. Appl.* **2**

[40] Wang Y, Cai W, Yang M, Liu Z and Shang G 2015 The simulation study of the plasmonic coupling effect for the Ag nanoparticle-nanowire structure *J. Korean Phys. Soc.* **66** 261–5

[41] Lal S, Hafner J H and Halas N J 2012 Noble Metal Nanowires : From Plasmon *Acc. Chem. Res.* **45** 1887–95

[42] Cao Z, He Y, Cheng Y, Zhao J, Li G, Gong Q and Lu G 2016 Nano-gap between a gold tip and nanorod for polarization dependent surface enhanced Raman scattering *Appl. Phys. Lett.* **109**

[43] Gu F, Zeng H, Tong L and Zhuang S 2013 Metal single-nanowire plasmonic sensors. *Opt. Lett.* **38** 1826–8

[44] Fu M, Qian L, Long H, Wang K, Lu P, Rakovich Y P, Hetsch F, Susha A S and Rogach A L 2014 Tunable plasmon modes in single silver nanowire optical antennas characterized by far-field microscope polarization spectroscopy *Nanoscale* **6** 9192–7

[45] Dorfmüller J, Vogelgesang R, Khunsin W, Rockstuhl C, Etrich C and Kern K 2010 Plasmonic nanowire antennas: Experiment, simulation, and theory *Nano Lett.* **10** 3596–603

[46] Song M, Chen G, Liu Y, Wu E, Wu B and Zeng H 2012 Polarization properties of surface plasmon enhanced photoluminescence from a single Ag nanowire *Opt. Express* **20** 661–5

[47] Miljković V D, Shegai T, Johansson P and Käll M 2012 Simulating light scattering from supported plasmonic nanowires. *Opt. Express* **20** 10816–26

[48] Panaretos A H and Werner D H 2015 A reduced order admittance model for longitudinally loaded plasmonic nanorod antennas *IEEE Antennas Propag. Soc. AP-S Int. Symp.* **2015**–**Octob** 262–3

[49] Song M, Dellinger J, Demichel O, Buret M, Colas Des Francs G, Zhang D, Dujardin E and Bouhelier A 2017 Selective excitation of surface plasmon modes propagating in Ag nanowires *Opt. Express* **25** 9138

[50] Ringe E, Sharma B, Henry A-I, Marks L D and Van Duyne R P 2013 Single nanoparticle plasmonics *Phys. Chem. Chem. Phys.* **15** 4110

[51] Goel P, Singh K and Singh J P 2014 Polarization dependent diffraction from anisotropic Ag nanorods grown on DVD grating templates by oblique angle deposition *RSC Adv.* **4** 11130

[52] Yang M, Cai W, Wang Y, Sun M and Shang G 2016 Orientation-and polarization-dependent optical properties of the single Ag nanowire/glass substrate system excited by the evanescent wave *Sci. Rep.* **6** 1–10

[53] Kabakova I V., De Hoogh A, Van Der Wel R E C, Wulf M, Le Feber B and Kuipers L 2016 Imaging of electric and magnetic fields near plasmonic nanowires *Sci. Rep.* **6** 1–9

[54] Rossouw D, Couillard M, Vickery J, Kumacheva E and Botton G A 2011 Multipolar plasmonic resonances in silver nanowire antennas imaged with a subnanometer electron probe *Nano Lett.* **11** 1499–504

[55] Gruber C, Hirzer A, Schmidt V, Trügler A, Hohenester U, Ditlbacher H, Hohenau A and Krenn J R 2015 Imaging nanowire plasmon modes with two-photon polymerization *Appl. Phys. Lett.* **106** 10–3

[56] Marquestaut N, Talaga D, Servant L, Yang P, Pauzauskie P and Lagugné-Labarthet F 2009 Imaging of single GaN nanowires by tip-enhanced Raman spectroscopy *J. Raman Spectrosc.* **40** 1441–5

[57] Livneh T, Zhang J, Cheng G and Moskovits M 2006 Polarized Raman scattering from single GaN nanowires *Phys. Rev. B* **74** 35320

[58] Kakko J, Matikainen A, Autere A and Kujala S 2017 Measurement of Nanowire Optical Modes Using Cross-Polarization Microscopy *Sci. Rep.* **7** 1–9

[59] Wiecha P R, Cuche A, Arbouet A, Girard C, Colas Des Francs G, Lecestre A, Larrieu G, Fournel F, Larrey V, Baron T and Paillard V 2017 Strongly Directional Scattering from Dielectric Nanowires *ACS Photonics* **4** 2036–46

[60] Polenta L, Rossi M, Cavallini A, Calarco R, Marso M, Meijers R, Richter T, Stoica T and Lüth H 2008 Investigation on Localized States in GaN Nanowires Investigation on

Localized States in GaN Nanowires **2** 287–92

[61] Ullah K, Liu X, Jichuan X, Hao J, Xu B, Jun Z and Liu W 2017 A Polarization Parametric Method of Sensing the Scattering Signals From a Submicrometer Particle *IEEE Photonics Technol. Lett.* **29** 19–22

[62] Liu X, Qiu B, Chen Q, Ni Z, Jiang Y, Long M and Gui L 2014 Characterization of graphene layers using super resolution polarization parameter indirect microscopic imaging *Opt. Express* **22** 20446

[63] Glazer A M, Lewis J G and Kaminsky W 1996 An automatic optical imaging system for birefringent media *Proc. R. Soc. London Ser. a-Mathematical Phys. Eng. Sci.* **452** 2751–65

[64] Kaminsky W, Claborn K and Kahr B 2004 Polarimetric imaging of crystals. *Chem. Soc. Rev.* **33** 514–25

[65] Nabi G, Cao C, Hussain S, Khan W S, Mehmood T, Usman Z, Ali Z, Butt F K, Fu Y, Li J and Iqbal M Z 2012 Photoluminescence and hydrogen storage properties of gallium nitride hexagonal micro-bricks *Mater. Lett.* **79** 212–5

[66] Nabi G, Cao C, Khan W S, Hussain S, Usman Z, Safdar M, Shah S H and Khattak N A D 2011 Synthesis, characterization, growth mechanism, photoluminescence and field emission properties of novel dandelion-like gallium nitride *Appl. Surf. Sci.* **257** 10289–93